Investigating the repeatability and behavioral relationships of acuity, contrast sensitivity, form, and motion perception measurements using a novel tablet-based vision test tool

Jonathan Green [1], Jan Skerswetat *[2,3], Peter J. Bex [3], Gunnar Schmidtmann [1]

[1] School of Health Professions, University of Plymouth, Plymouth, United Kingdom
[2] Department of Psychology, Northeastern University, 360 Huntington Ave, Boston, Massachusetts, 02115, United States of America
[3] Department of Ophthalmology, University of California, 850 Health Sciences Road, Irvine, California, 9269, United States of America

Jonathan Green: https://orcid.org/0000-0001-5738-7515
Jan Skerswetat: https://orcid.org/0000-0002-2470-8404
Peter J. Bex: https://orcid.org/0000-0001-7561-7695
Gunnar Schmidtmann: https://orcid.org/0000-0001-8180-7751

*Corresponding author email: jskerswe@hs.uci.edu
Emails: jon.green@plymouth.ac.uk, jskerswe@hs.uci.edu, p.bex@northeastern.edu, gunnar.schmidtmann@plymouth.ac.uk

Abstract (280 words)

Visual function tests are important in basic and clinical vision research but are typically limited to very few aspects of human vision, coarse diagnostic resolution, and require an administrator. Recently, the generalizable, response-adaptive, self-administered Angular Indication Measurement (AIM) and Foraging Interactive D-prime (FInD) methods were developed to assess vision across different visual functions. The AIM and FInD paradigms show a range of visual stimuli per display (4x4 stimuli) spanning ±2σ around an adaptively estimated perceptual threshold across multiple displays. Here, we investigated the repeatability and behavioral relationships of the AIM and FInD paradigms for near visual acuity, contrast sensitivity function (CSF), form, and motion coherence threshold measurements using a novel tablet-based vision test tool. 31 healthy participants were recruited and completed two repetitions of each experiment in random order. Bland-Altman analyses were performed to calculate the Coefficient of Repeatability (precision) and Mean Bias (accuracy). Linear regressions and hierarchical cluster analysis were used to investigate the relationship between outcome parameters. Results show that AIM Form coherence and FInD Form horizontal coherence showed significant retest bias; all other tests were bias-free. Cluster analysis revealed overall clustering of CSF, form and motion outcomes. We further show significant correlations within CSF and between motion coherence outcomes but few significant correlations between form coherence outcomes. AIM and FInD near vision tests are generalizable across multiple visual functions and are precise and reliable. Most functions tested were

bias-free. CSF, form, and motion outcomes clustered together, and CSF and motion outcomes correlated with one another. The combination of a generalizable, response-adaptive, and self-administered approach may be a suitable set of tests for basic science and clinical use cases.

Keywords: visual acuity, contrast sensitivity, form perception, motion perception, psychophysical methods, response-adaptive, self-administered, tablet-based, vision test, angular indication measurement, foraging interactive D-prime, repeatability

Introduction

Identification and measurement of visual dysfunction is a global challenge. In excess of 1 billion people have visual impairments that could have been or are yet to be addressed (World Health Organisation (WHO), 2019; Bourne *et al*., 2019) with the estimated associated loss of productivity valued at US$ 410.7 billion (WHO, 2023). This challenge is exacerbated by the disproportionate prevalence of visual deficiency in lower and middle-income countries (90%) (WHO, 2023; Rizzo *et al*., 2020; WHO, 2022) and in higher income countries, amongst those from ethnic minorities, with lower socio-economic status, lower educational attainment (Cumberland *et al*. 2016; Elam *et al*. 2022), and poorer general and mental health (Cumberland *et a*l. 2016). Ageing is also strongly associated with increased risk for many visual conditions (Killeen *et al*., 2023; Martinez-Roda *et al.*, 2016) - including subtle and under-recognised presentations, such as those often associated with mild traumatic brain injury (Rasdall *et al*., 2024) (over 1-million annually in the US alone). Globally, the number of people aged over 65 is predicted to double over the next quarter of a century (United Nations, 2022), representing a substantial generator of pressure on often already overstretched health services.

Innovative digital technologies offer a range of opportunities to mitigate such challenges (Chen, Ding & Wang, 2023). Many digital vision assessment tools are available, some of which can now be operated using conventional portable devices such as laptop and tablet computers, or even smartphones (Bano, Wolffsohn & Sheppard, 2024). Advances in functionality support rapid, non-specialist, point-of care and domiciliary assessment, as well as self-administration and remote operation (telemedicine, Samanta *et al.*, 2023). These technologies promise to drive more efficient assessment and monitoring, at earlier disease stages, reducing inconvenience and expense, and increasing access to underserved patient groups (Khurana *et al*., 2021). As yet, these novel systems generally target a limited range of visual functions – and many are yet to be subjected to robust, peer-reviewed validation of their accuracy and reliability (Bano, Wolffsohn & Sheppard, 2024).

This study focuses on new ‘Perzeption’ suites of computer-based visual assessment tools which apply novel psychophysical paradigms and algorithms; namely the Angular Indication Measurement (AIM) (Skerswetat *et al.*, 2024a; Neupane, Skerswetat & Bex, 2024) and the Foraging Interactive D-prime (FInD) (Bex & Skerswetat, 2021; He, Bex & Skerswetat, 2023; Skerswetat *et al*., 2024b). Tests employing these generalisable, self-administered, multi-dimensional (spatial/temporal frequency/contrast), and response-adaptive (personalised) psychophysical methods have been developed to measure more than 15 visual functions (Skerswetat *et al.*, 2024b) including visual acuity with and without glare source (Skerswetat, Boruta & Bex, 2022), colour (He, Bex & Skerswetat, 2023) and depth perception (Neupane, Skerswetat & Bex, 2024), spatio- and spatio-temporal contrast sensitivity (Skerswetat *et al*., 2024b), threshold versus contrast

suprathreshold perception (Bex & Skerswetat, 2021; Bex & Skerswetat, 2023), form and motion perception (Bex & Skerswetat, 2021; Skerswetat *et al*., 2024b; Merabet *et al*., 2023), and face discrimination (Walter & Bex, 2024). Advantages of these methods compared to traditional clinical tests and current laboratory computer-based methods include flexible testing ranges, fine outcome resolution and improved detection of subtle changes, a bias-free test protocol due to randomised stimulus orientations and variables that eliminate memorisation risks, rapid testing through adaptive algorithms and instant result generation, reduction in administrative burden and time due to self-administration, and a generalizable method to measure multiple visual functions using the same principal, i.e., orientation judgement for AIM and signal presence detection for FInD.

The AIM method can be applied with different stimulus and response formats, generating orientation judgements. Psychometric functions are fit to continuous orientation report errors (as a function of stimulus intensity) (Skerswetat *et al*., 2024a). The FInD method measures the identification of cells containing signal stimuli of varying intensities, amongst null stimuli cells. Thresholds are estimated from *d'* analysis of hits, misses, false alarms, and correct rejection responses (Skerswetat *et al*., 2024b).

Previous studies have supported the refinement and administration of many of these assessment tools. One study demonstrated the systematic application of a battery of eleven tests, across both paradigms, for the broad visual assessment of 21 research participants with visual dysfunction (people with albinism), compared with 21 typically sighted controls (Skerswetat *et al*., 2024b). Anticipated variance between groups was observed – and the incorporation of testing pertinent to different levels of visual processing provided insight into a lack of differentiation for some mid-level functioning (pattern recognition, and radial and circular motion coherence). The FInD global motion coherence test has also been demonstrated to identify an anticipated significant reduction in performance amongst a cohort of 20 young people with cerebral visual impairment, compared with 30 controls (mean difference 32.34%) - concurrently providing evidence of usability by neurodiverse participants and for the targeted assessment of cerebral visual processing (Merabet *et al*., 2023). Participants were able to use both form and motion tests, taking an average of around 6 minutes to complete both.

In a study of 22 young adults with induced defocus and astigmatic blur, results from the AIM visual acuity (VA) test demonstrated comparable sensitivity to conventional Early Treatment Diabetic Retinopathy Study (ETDRS) letter chart assessment and comparable repeatability when the AIM test includes three adaptive steps (mean VA test retest bias 0.03 and 0.02, respectively), whilst providing additional personalised information regarding minimal error level (noise), bias and slope from a psychometric function fit (Skerswetat *et al*., 2024a). Mean AIM VA test duration was only around 30 seconds. Elsewhere, a study of 24 children (including 11 amblyopes)

demonstrated the usability of AIM VA for children as young as 5 years, taking an average of around 1.5 minutes (Ahmed *et al.*, 2023). The results demonstrated good agreement with Snellen and Rosenbaum chart use (ANOVA group effect = 0.612) and identified interocular VA differences.

The AIM Contrast Sensitivity Function (CSF) test was appraised in a study of 10 participants (8 typically sighted, 1 amblyopic and 1 Ortho-K contact lens wearer with defocus blur) (Skerswetat & Bex, 2022). Between-eye results were similar, and less than for both eyes together, consistent with binocular contrast summation. Anticipated interocular difference and overall performance reduction was observed for the respective atypically sighted participants. CSF testing was generally completed within 2 minutes. Elsewhere, results of FInD CSF and Threshold versus Contrast functions (TvC) [stereoacuity, spatial coherence and motion coherence] tests were found to be comparable to the results of equivalent standard temporal two-alternative forced choice (2-AFC) paradigms for up to 14 participants (Bex & Skerswetat, 2021). The FInD tests were significantly quicker to administer, and no significant test retest difference or *bias* were detected.

Whilst this is a test retest study, it is of note that there is also an accumulation of evidence regarding the performance of other tests in the Perzeption batteries compared to established measures. The AIM Threshold versus Contrast (TvC) and Equivalent Noise (EN) assessments for form, motion and color have been demonstrated to be comparable to two-alternative forced choice (2-AFC) tests (Bex & Skerswetat, 2023). Elsewhere, both FInD and AIM tests for stereopsis reliably detected deficits compared to 2-AFC and Titmus and Randot clinical tests, although stereo thresholds were 1.3-1.6 times higher for FInD and 2-AFC than for the clinical tests (Neupane, Skerswetat & Bex, 2024). Regarding color vision assessment, FInd and AIM tests agreed well with Cambridge Color Test (CCT) thresholds and Mollon-Reffin scores for the detection of color vision deficiency (CVD). AIM and FInD performance slightly reduced for CVD categorisation, but their combined results were comparable to the other tests (Arthur *et al*., 2025). The FInD test reliably categorised CVD compared to Hardy-Rand-Rittler and Farnsworth-Munsell 100 hue tests, accepting that even the results of these two other methods were not entirely uniform (He, Bex & Skerswetat, 2023) and in another study the AIM test was demonstrated to have good agreement with anomaloscope readings for CVD detection (He, Skerswetat & Bex, 2023).

Performance across visual perception domains does not appear to be highly correlated in healthy adults, suggesting multifactorial determinants of normal visual function (Tulver, 2019). Attempts to map consistent relationships between potentially associated sub-groups of functions have also, as yet, only yielded modest correlations (Bosten *et al*., 2017a; Cappe et al., 2014; Herzog *et al.*, 2025; Shakiri *et al*., 2019). Intra-observer variance appears to be stable over time, i.e. consistently deteriorating (Garobbio, Kunchulia & Herzog, 2014), and certain traits may be

associated with specific disorders (Bosten *et al*., 2017b). The inherent efficiency and the relative homogeneity of interface, stimulus type, format, etc. of this test battery may prove useful in the advancement of research in this field.

The aim of the current study is to investigate the repeatability and behavioral relationships of the AIM and FInD paradigms for acuity, contrast sensitivity, form, and motion perception measurements implemented as a novel tablet-based vision test tool.

Methods

Participants

31 observers (mean age: 39.7, σ: ±11.7; 13 females) participated in the initial test-retest study. Seven additional observers (mean age: 39, σ: ±15; 4 females) were recruited for a control experiment (AIM CSF with five displays, see details below). 36 observers were naive as to the purpose of the experiment. All participants had normal or corrected-to-normal visual acuity. To assess whether performance in the visual tests was influenced by Asperger syndrome (i.e., high-functioning autism) or attention deficit hyperactivity disorder (ADHD), all participants completed the Adult ADHD Self-Report Scale (ASRS; Kessler et al., 2005) and the Autism-Spectrum Quotient (AQ; Baron-Cohen et al., 2001) questionnaires (see Table 1 caption for details). Participants also provided information regarding their medical history. One participant reported hemiplegic migraines, three reported past (non-recent) concussions, one reported anxiety, emotional dysregulation, and depression, and another had a diagnosis of dyslexia. None of these conditions were considered sufficient grounds for exclusion. Reported ocular conditions (e.g., myopia, astigmatism) did not affect participant eligibility, as all tests were conducted with appropriate visual correction. Likewise, reported colour vision deficiencies were not considered exclusionary, since none of the tasks involved coloured stimuli. Informed, written consent was obtained from each observer, and the study was approved by the University of Plymouth ethics committee. All experiments were conducted in accordance with the Declaration of Helsinki.

Table 1 Self-reported participant demographic and medical details. Ethnicity: White (UK, Irish) includes English, Welsh, Scottish, Irish, British. Sex: f = female; m = male. ADHD & Autism Thresholds: Adler's Adult ADHD Self-Report Scale (ASRS-v1.1). Part A (screener) ≥ 4 grey boxes = highly consistent with ADHD; Baron-Cohen's Autism Spectrum Quotient (AQ): ≥32 = Clinically significant (80% of those diagnosed with autism, but <2% of controls), ≥ 26 = Potential traits

ID	Age	Ethnicity	Sex	Medical history	Ocular conditions	ASRS	AQ
1	48	White (UK, Irish)	m		Myopia	0	20
2	44	White (UK, Irish)	m			0	14
3	48	White (UK, Irish)	m	Hemiplegic migraine	Astigmatism	1	23
4	22	Black	m			0	11
5	44	White (UK, Irish)	f			0	7
6	35	White (UK, Irish)	f			2	15
7	42	White (UK, Irish)	m	Concussion		1	18
8	49	White (UK, Irish)	m			0	23
9	39	White (UK, Irish)	m			0	11
10	29	White (UK, Irish)	f	Anxiety, Emotional dysregulation, Depression		3	10
11	28	White (UK, Irish)	m			2	22
12	23	Asian	m		Color-Vision-Defect	0	12
13	20	Black	f			0	17
14	28	White (UK, Irish)	f			2	10
15	28	White (UK, Irish)	m			5	39
16	48	White (UK, Irish)	m			2	21
17	26	Asian	m			2	25
18	32	White (UK, Irish)	m	Concussion		3	28
19	29	White (UK, Irish)	m	Concussion		2	21
20	19	White (UK, Irish)	f			2	12
21	57	White (UK, Irish)	f			0	11
22	54	White (any other)	f			0	10
23	48	White (UK, Irish)	f	Dyslexia		2	14
24	43	White (UK, Irish)	m			2	20
25	58	White (UK, Irish)	f			1	15
26	35	White (UK, Irish)	m			0	8
27	50	White (UK, Irish)	f		Astigmatism	0	15
28	55	White (UK, Irish)	f			2	24
29	46	White other)	m			0	13
30	51	White (UK, Irish)	f			0	10
31	40	mixed	m			0	30

Stimuli and psychophysical procedure

Each display chart for each test contained a 4x4 set of cells. All tests used three charts per experimental run, including the first initial chart and two adaptive steps for all tests. The range of stimulus test levels on each display spanned ±2σ around an adaptively estimated perceptual threshold across displays (e.g., Skerswetat *et al.*, 2024b; Skerswetat, Boruta & Bex, 2022). For form and motion perception testing, the default display mode, which presents all stimuli simultaneously and also the hidden cell approach, which shows only the stimulus over which the user positions the cursor (Merabet *et al.*, 2023) was used. Orientations or directions of stimuli within cells were randomized for all AIM tests. Stimulus examples are shown in Figure 1.

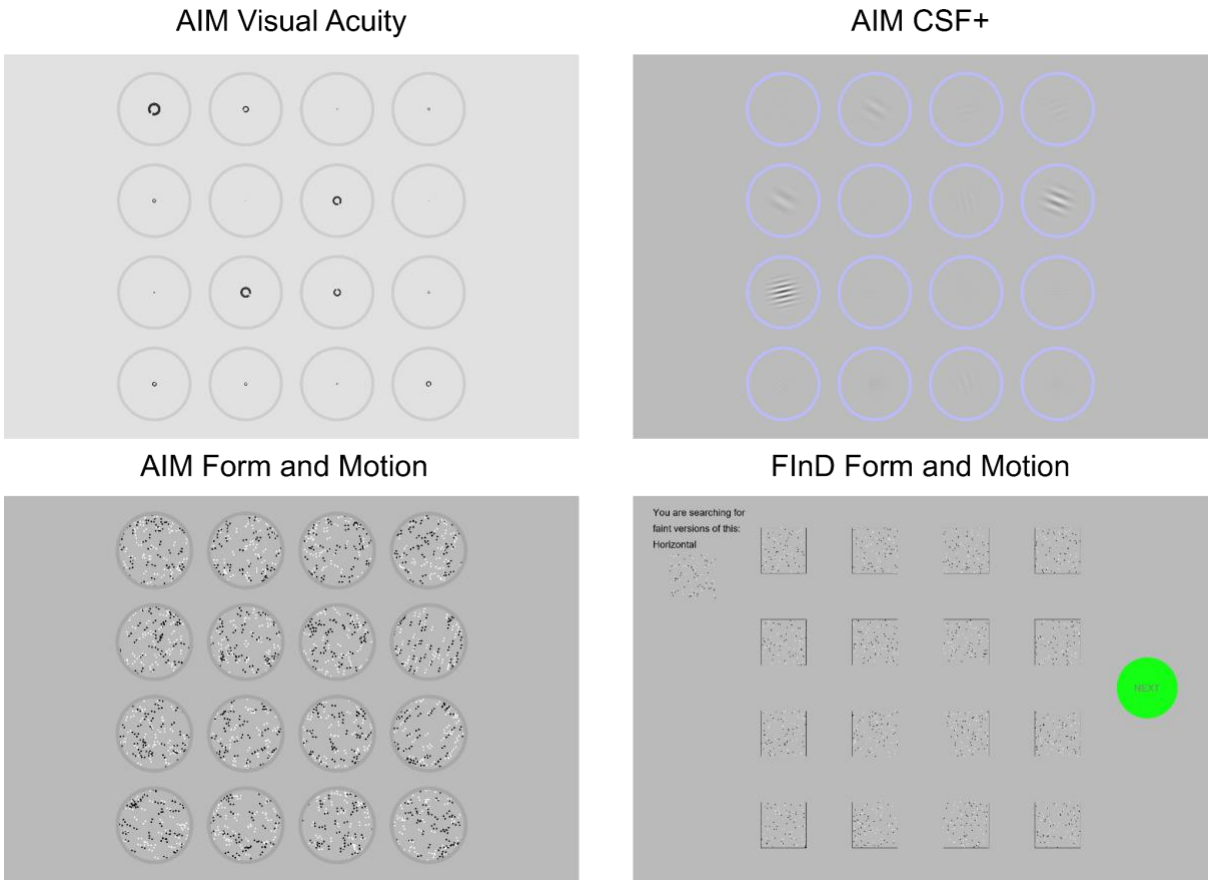

Figure 1 The images show charts containing stimulus examples for the AIM Visual Acuity (VA), AIM CSF+, AIM Form and Motion Coherence and FInD Form and Motion Coherence tests as seen by the observers on the tablet.

Angular Indication Measurement (AIM)

Participants indicated the perceived orientation of all 16 stimuli on one chart by clicking on each surround ring (see Figures 1 and 2) or making their best guess if they were not sure. The testing time was unlimited, and correction of indications were permitted prior proceeding to the next chart by clicking on a 'Next' button that became available only once responses had been made to all 16 stimuli (see bottom right in Figure 1). The response error was calculated as the absolute angular difference between target orientation and indicated orientation. After the final chart was completed, a cumulative Gaussian function was fit to the absolute angular error data as a function of stimulus intensity, namely optotype size (AIM-VA), grating contrast (AIM CSF+), translational form or motion coherence (AIM-Form and AIM-Motion) from all charts, defined as

$$\tau_\theta(s) = \theta_i + \left(\theta_{guess} - \theta_i\right) \cdot \left(0.5 - 0.5 \cdot erf\left(\frac{s-\tau}{\sqrt{2\gamma}}\right)\right), \quad (1)$$

where θ_{guess} denotes the orientation error for a guess response (the absolute orientation error of random responses for stimuli is uniformly distributed with a mean of 90° for Landolt C optotypes, translation form and motion coherence). For Gabors during AIM-CSF2d+, the rotational symmetry θ_{guess} is 45°. s denotes the signal intensity, τ a sensitivity threshold, θ_i is internal angular uncertainty, the absolute angular report error for the most visible stimulus, which we refer to as a *noise* parameter as it is due to some of the ex- and internal noise sources, and γ is the slope of the psychometric function.

AIM Acuity: Landolt C optotypes were presented within each indication ring (diameter, Ø: 5°) with an inter-cell distance of 1°. Stimulus contrast was 0.97. The minimum range of stimuli sizes was set to 0.20 logMAR. The minimum visual acuity was kept at the minimum renderable size for -0.05 logMAR and maximum logMAR starting value was set to 1.00 logMAR. More details are published elsewhere (Skerswetat *et al*., 2024a).

AIM Form Coherence (with and without Hidden Cells): Glass Pattern (Glass, 1969; Glass & Perez, 1973) coherence for translational form coherence was measured with 100 dipoles (50 black, 50 white; cell Ø: 5°; dot Ø=0.1°; intra-dipole spacing=0.2°).

AIM Motion Coherence (with and without Hidden Cells): Motion coherence for translational global dot motion was measured. Each cell (Ø: 5°) contained 100 black or white dots (Ø=0.1°, lifetime=100ms with random starting age, speed=2°/sec, dot contrast: 1.0). Stimulus examples are presented in the supplementary AIM_Motion.mp4 video file.

AIM CSF 2D+: Gabors (σ: 0.5°) were presented within each indication ring (Ø: 5°) with an inter-cell distance of 1˚.
One initial and two adaptive charts were presented and the task was to click on the ring surrounding each Gabor to indicate the orientation of the grating or to make a guess (Figure 2). We assessed the CSF acuity (high spatial frequency cutoff) and the area under the *log*CSF (AULCSF). In order to increase the greyscale resolution of the 8-bit monitor, we applied the noisy-bit binomial sampling method (Allard & Faubert,2008).
The angular report errors were fit with an asymmetric *log* parabola to estimate the CSF.

$$f(SF) = \begin{cases} CS_p - \left(SF - SF_p\right)^2 \cdot (width_L)^2 & if\ SF < SF_p \\ CS_p - \left(SF - SF_p\right)^2 \cdot (width_R)^2 & if\ SF \geq SF_p \end{cases}, \quad (2)$$

The variable *CSp* denotes the peak contrast sensitivity, *SFp* the peak spatial frequency, and $width_L$ and $width_R$ are the lower and upper bandwidths (Watson & Ahumada, 2005).

AIM specific feedback: Auditory feedback was provided after each chart based on a statistical probability analysis of per-chart report errors. If the mean error report was indistinguishable from random responses (i.e., 90° error for C optotypes and motion directions, 45° for gratings and Glass patterns), the application altered the user to report the orientation carefully.

Foraging Interactive D-prime (FInD)

The right panel in Figure 2 illustrates the FInD method. The task for the participants was to select cells for each chart that contained a stimulus. No time-constraint was given. Selected cells could be unselected within each chart and were only locked after pressing the green “Next” button to initiate the next display (see bottom right in Figure 1). The response in each cell was categorised as either Hit, Miss, False Alarm, or Correct Rejection, to calculate *d’,* and the probability of a Yes response as a function of signal intensity was calculated according to

$$p(Yes) = 1 - \phi \cdot \left(\phi^{-1}(1 - F) - \frac{d'_{max} \cdot \left(\frac{S}{\theta}\right)^{\gamma}}{\sqrt{\left(\left(d'_{max}\right)^2 - 1\right) + \left(\frac{S}{\theta}\right)^{2\gamma}}} \right), \quad (3)$$

where *p(Yes)* is the probability of a Yes response, ϕ is the normal cumulative distribution function, and *F* is the false alarm rate, *S* denotes the stimulus intensity, θ the threshold, d'_{max} is the saturating value of *d’* (fixed at 5), and γ is the slope. The fit to data from all completed charts was used to select the individualized range (i.e., *d’*

= 0.1 to 4.5) of stimulus intensities (namely static Glass (Glass & Perez,1973) or motion coherence patterns) for subsequent charts.

FInD Form (with and without Hidden Cells): Glass Pattern coherence (Merabet *et al*., 2023; Glass, 1969; Glass & Perez, 1973) for translational, circular, and expanding (radial) form coherence was measured with 100 dipoles (50 black, 50 white; cell Ø: 3x3° squares; dot Ø=0.05°; inter-dot spacing=0.2°). The inter-cell distance was 3°.

FInD Motion (with and without Hidden Cells): Global motion coherence (Merabet *et al*., 2023) for translational, circular, and expanding form coherence was measured with 100 dipoles (50 black, 50 white; dot contrast: 1.0; cell Ø: 3*3° squares; dot Ø=0.05°; speed=1°/sec, lifetime=100ms with random starting age). The inter-cell distance was 3°.

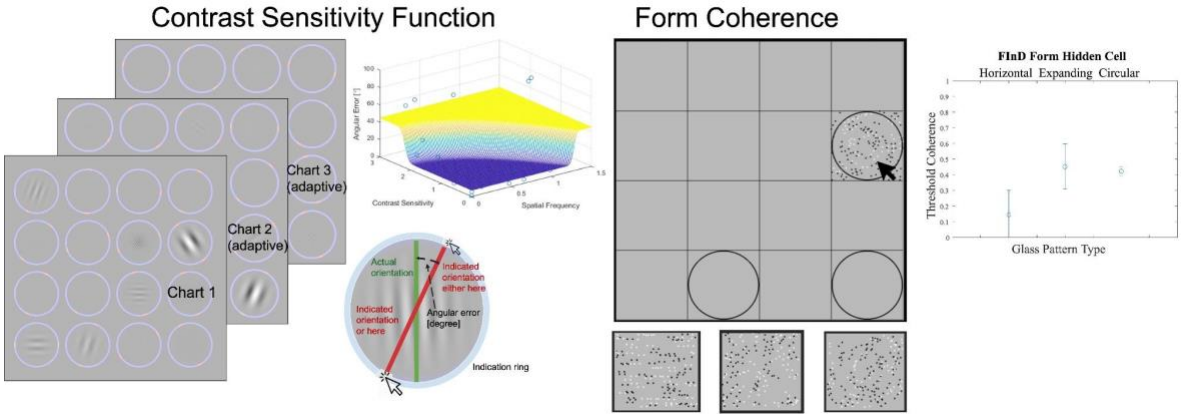

Figure 2: Schematic illustration of the AIM (left) and FInD (right) methods. Left: The AIM method is exemplified by the AIM-CSF 2D+ paradigm. The initial chart showed Gabor patches with a range of different spatial frequencies and contrasts. Participants then indicate the perceived orientation of each Gabor or make their best guess before continuing to the next chart by pressing a green "Next button" that appears after all 16 indications are made (not shown here). Subsequent charts adaptively homing in around the CSF. After completing the final chart, the *log* parabola function was fit to the absolute report errors to estimate the area under the log CSF and CSF-acuity. The difference between the actual Gabor orientation (green line) and indication orientation (red line) are shown underneath the example fit. The right illustration shows the FInD Form using the hidden cell method. The initial chart contains 16 cells, 9-12 of them contain a signal (e.g., circular Glass patterns) of varying intensities (randomly positioned within the chart), and all other cells contain noise. The participant uses a computer mouse to hover over each cell to make it appear, judges whether it is a signal and makes their indication before moving to the next cell. The participant was instructed to "zigzag" over each cell before clicking on the "Next" button, which contained a different form-coherence (horizontal, expanding, circular in random order). Once the first initial chart for each form coherence type was completed, the next charts adaptively converged on ±2 standard deviation around each form pattern threshold and then repeated until three charts per form coherence type were completed. The psychometric functions and their 95% confidence intervals (CI) were fit to each form coherence type. An example outcome for FInD Form thresholds and 95% CIs is depicted on the right.

Correlation and cluster analysis

Python, including the Seaborn toolbox (Waskom, 2021) was used to perform and visualize the linear correlation and hierarchical cluster analysis. Data were normalized using z-score normalization. The marginal cluster trees show a hierarchical cluster analysis using Ward's Minimum Variance Clustering Method based on the Euclidean distance between objects (i.e., test results). Linear correlations using Kendall coefficients were used.

Apparatus

Stimuli were presented on a Microsoft Surface Pro 8 (Core^{TM} i5 CPU 8GB, 256GB Go RAM) with display dimensions of 27.4 x 18.3 cm. The display's spatial resolution was 2880 x 1920 pixels with a 60Hz frame rate. All experiments were carried out at a viewing distance of 40 cm. The experimenter monitored the viewing distance throughout the task and provided feedback if the viewing position was changed. Note that while participant responses are therefore self-administered and data analysis was automated, monitoring of viewing distance therefore involved supervision by the examiner. At this distance, one pixel subtends 0.0136° visual angle. The screen was gamma-corrected using data color Spyder (Datacolor, Lucerne, Switzerland) photometer. The input for the AIM tests was via the tablet's touchscreen. The AIM hidden cell and FinD paradigm reports were made using a common computer mouse.

Procedure

Repeatability of near visual acuity, contrast sensitivity function (CSF), and form & motion coherence tasks were deployed on a tablet (see above). Observations were made under binocular viewing conditions. The test order was randomised, each experiment included a test and a retest session and took in total ~90 min.

Results

Psychophysical outcomes

The PerZeption application generated automatically outcomes as described below.

AIM: A cumulative Gaussian function (equation 1) was fit to the data of the AIM Visual Acuity, AIM Form Coherence, and AIM Motion Coherence tests (Neupane *et al.*, 2024; Skerswetat *et al.*, 2024b). Threshold, slope, and minimum report error parameter were calculated. For the AIM CSF 2D+, the area under the log CSF (AULCSF) and the high spatial frequency cut off, or CSF Acuity were analysed.

FInD: Response of each cell was classified as either Hit, Miss, False Alarm, or Correct Rejection, to calculate *d'* as a function of motion or form coherence. The probability of a Yes response as a function of signal intensity was subsequently calculated (equation 3, Merabet *et al.*, 2023). Threshold (*d'*=1), slope, and false alarm rate parameters were calculated.

Bland-Altman Analysis

Test-retest reliability for all tests was assessed using Bland-Altman (Altman & Bland, 1983) plots using MATLAB (R2024b, Matworks). Figure A1 in the appendix shows an example (see Supplementary Material for all Bland-Altman plots).

We subsequently calculated the Coefficient of Repeatability (precision, *CoR*) according to

$$CoR = 1.96\sqrt{2}\sigma, \quad (4)$$

where σ refers to the within-subject standard deviation. The mean bias ($\underline{x}_{bias}$, accuracy) in Table 2 was calculated as

$$\underline{x}_{bias} = \frac{\sum_{i=1}^{n} (m_{1i} - m_{2i})}{n}, \quad (5)$$

where m_1 and m_2 denote the test and retest measurements, respectively. One-sample t-tests were conducted to assess whether the bias is statistically significant. Test-retest data (m_1, m_2), *CoR*, mean *Bias* and *p*-values are summarized in Table 2, where $p \leq 0.05$ is considered statistically significant and indicated by asterisks.

Results show that AIM Form coherence results and FInD Form horizontal coherence results showed significant retest biases, but all other tests were bias-free.

421 **Table 2** Test Retest results for threshold values (Coh. = coherence threshold, HC = hidden cell mode,
422 σ = standard deviation, *CoR* = coefficient of repeatability).

Visual function test	Basic Statistics		Bland-Altman Statistics		
	Test (m_1) Mean ±σ	**Retest (m_2) Mean ±σ**	***CoR***	**Mean *Bias***	**Mean *Bias p***
AIM-VA [logMAR] (*fixed at limit (-0.104))	-0.06 ±0.05	-0.06 ±0.06	±0.19	-0.001	*p*=.94
AIM CSF+: AULCSF (3 charts) 5 charts *fixed at limit	2.55 ±0.54 3.00 ±0.014	2.41 ±0.52 2.98 ±0.066	±1.68 ±0.14	0.14 0.02	*p*=.21 *p*=.36
AIM CSF+: Acuity (3 charts) [c/°]	26.0 ±5.8	23.7 ±5.9	±20.1	2.3	*p*=.09
5 charts *fixed at limit	30.9 ±0.00	30.6 ±0.79	±2.26	0.3	*p*=.36
AIM-Form Coh. [%]	44.6 ±24.3	36.9 ±20.3	±44.8	7.6	*p*=.013*
AIM-Form Coh. [%] Hidden cell mode	49.9 ±27.7	44.5 ±24.7	±66.5	5.4	*p*=.21
AIM-Motion Coh. [%]	41.8 ±27.3	41.5 ±27.2	±85.3	0.3	*p*=.96
AIM-Motion Coh. [%] HC	41.2 ±28.3	40.4 ±28.3	±78.9	0.8	*p*=.87
FInD-Form Coh. - Horizontal [%]	41.1 ±25.8	32.4 ±22.7	±75.4	8.7	*p*=.08
FInD-Form Coh. - Expanding [%]	38.4 ±16.9	35.5 ±18.9	±75.0	2.8	*p*=.56
FInD-Form Coh. - Circular [%]	39.7 ±19.5	36.2 ±17.9	±61.8	3.5	*p*=.39
FInD-Form Coh. - Horizontal[%] HC	43.1 ±26.8	26.8 ±21.0	±68.3	16.0	*p*<.001***
FInD-Form Coh. - Expanding [%] HC	32.9 ±19.0	30.7 ±22.0	±72.3	2.2	*p*=.64
FInD-Form Coh. - Circular [%] HC	38.5 ±14.0	38.2 ±19.0	±58.4	0.3	*p*=.93
FInD-Motion Coh. - Horizontal [%]	25.6 ±19.5	35.3 ±25.5	±66.0	-9.7	*p*=.03*
FInD-Motion Coh. - Expanding [%]	31.3 ±15.5	33.7 ±15.7	±37.9	-2.4	*p*=.33
FInD-Motion Coh. - Circular [%]	19.1 ±12.9	22.4 ±15.8	±35.5	-3.3	*p*=.16
FInD-Motion Coh. - Horizontal [%] HC	21.3 ±19.8	27.2 ±25.5	±57.1	-6.0	*p*=.12
FInD-Motion Coh. - Expanding [%] HC	32.7 ±18.8	33.2 ±18.7	±59.4	-0.5	*p*=.89
FInD-Motion Coh. - Circular [%] HC	18.3 ±11.7	20.1 ±13.0	±29.1	-0.02	*p*=.35

423
424
425
426
427
428
429
430

Table 3 Test Retest results for slope values.

Slopes	**Test (m_1) Mean ±σ**	**Retest (m_2) Mean ±σ**	***CoR***	**Mean *Bias***	**Mean *Bias p***
AIM-VA	0.12 ±0.12	0.12 ±0.13	0.49	-0.01	*p*=.8694
AIM CSF+: AULCSF (3 charts)	0.34 ±0.11	0.26 ±0.14	0.46	0.08	*p*=.0169*
AIM CSF+ Acuity (3 charts)	0.34 ±0.11	0.26 ±0.14	0.46	0.08	*p*=.0169*
AIM-Form Coh.	0.20 ±0.15	0.17 ±0.13	0.50	0.03	*p*=.3597
AIM-Form Coh. HC	0.23 ±0.18	0.21 ±0.17	0.56	0.01	*p*=.6926
AIM-Motion Coh.	0.16 ±0.16	0.12 ±0.11	0.47	0.04	*p*=.2310
AIM-Motion Coh. HC	0.16 ±0.13	0.14 ±0.12	0.50	0.02	*p*=.4814
FInD-Form Coh. - Horizontal	1.94 ±1.32	1.82 ±1.33	5.34	0.12	*p*=.7282
FInD-Form Coh. - Expanding	2.65 ±1.32	2.28 ±1.28	4.30	0.37	*p*=.1975
FInD-Form Coh. - Circular	2.63 ±1.22	2.16 ±1.22	3.59	0.47	*p*=.0520
FInD-Form Coh. - Horizontal HC	1.99 ±1.14	1.71 ±1.29	5.50	0.28	*p*=.4380
FInD-Form Coh. - Expanding HC	2.31 ±1.41	1.88 ±1.34	5.13	0.43	*p*=.2064
FInD-Form Coh. - Circular HC	2.55 ±1.24	2.79 ±1.35	5.10	-0.24	*p*=.4704
FInD-Motion Coh. - Horizontal	2.34 ±1..49	2.55 ±1.47	5.42	-0.20	*p*=.5656
FInD-Motion Coh. - Expanding	2.55 ±1.24	3.03 ±1.13	4.47	-0.49	*p*=.1033
FInD-Motion Coh. - Circular	2.27 ±1.40	2.48 ±1.21	5.38	-0.22	*p*=.5349
FInD-Motion Coh. - Horizontal HC	1.95 ±1.33	2.14 ±1.39	5.81	-0.19	*p*=.6260
FInD-Motion Coh. - Expanding HC	2.84 ±1.15	2.78 ±1.43	4.45	0.06	*p*=.8306
FInD-Motion Coh. - Circular HC	2.61 ±1.29	2.53 ±1.34	4.27	0.08	*p*=.7628

Table 4 Test-retest results for minimum report errors values.

Errors [°]	Test (m_1) Mean ±σ	Retest (m_2) Mean ±σ	*CoR*	Mean *Bias*	Mean *Bias p*
AIM-VA	12.05 ±5.77	11.43 ±5.65	22.27	0.62	*p*=.6695
AIM CSF+: AULCSF	8.32 ±3.14	8.41 ±3.01	9.96	-0.09	*p*=.8900
AIM CSF+ Acuity	8.32 ±3.14	8.41 ±3.01	9.96	-0.09	*p*=.8900
AIM-Form Coh.	10.10 ±6.74	12.36 ±7.58	23.20	-2.26	*p*=.1430
AIM-Form Coh. HC	9.41 ±7.87	11.14 ±8.89	27.64	-1.73	*p*=.3410
AIM-Motion Coh.	15.94 ±15.71	15.40 ±15.80	47.84	0.54	*p*=.8631
AIM-Motion Coh. HC	16.29 ±13.39	13.25 ±15.78	53.69	3.04	*p*=.3894
FInD-Form Coh. - Horizontal	0.09 ±0.11	0.07 ±0.09	0.33	0.01	*p*=.5649
FInD-Form Coh. - Expanding	0.08 ±0.09	0.09 ±0.13	0.33	0.00	*p*=.8917
FInD-Form Coh. - Circular	0.04 ±0.07	0.07 ±0.08	0.15	-0.03	*p*=.0097*
FInD-Form Coh. - Horizontal HC	0.12 ±0.14	0.08 ±0.11	0.38	0.04	*p*=.0896
FInD-Form Coh. - Expanding HC	0.14 ±0.18	0.07 ±0.08	0.49	0.07	*p*=.0336*
FInD-Form Coh. - Circular HC	0.08 ±0.10	0.07 ±0.10	0.29	0.01	*p*=.4588
FInD-Motion Coh. - Horizontal	0.13 ±0.17	0.12 ±0.17	0.48	0.01	*p*=.8697
FInD-Motion Coh. - Expanding	0.05 ±0.07	0.03 ±0.06	0.23	0.02	*p*=.2093
FInD-Motion Coh. - Circular	0.04 ±0.07	0.07 ±0.14	0.24	-0.03	*p*=.0982
FInD-Motion Coh. - Horizontal HC	0.13 ±0.20	0.13 ±0.16	0.50	0.00	*p*=.8969
FInD-Motion Coh. - Expanding HC	0.08 ±0.09	0.08 ±0.13	0.29	0.00	*p*=.8124
FInD-Motion Coh. - Circular HC	0.03 ±0.04	0.05 ±0.13	0.33	-0.02	*p*=.3096

Table 5 Summary of overall testing time and per-chart time.

Visual function test	Total Duration [s]		Chart duration [s]	
	Test (m_1) Mean ±σ	**Retest (m_2) Mean ±σ.**	**Test (m_1) Mean ±σ**	**Retest (m_2) Mean ±σ**
AIM-Visual Acuity	109 ±40	92 ±34	36 ±13	31 ±11
AIM CSF+ (3 charts)	145 ±64	111 ±46	48 ±21	37 ±15
AIM- Form Coherence	196 ±111	177 ±21	65 ±40	59 ±82
AIM- Form Coherence HC	244 ±191	164 ±107	81 ±64	55 ±36
AIM- Motion Coherence	222 ±90	176 ±34	74 ±30	59 ±34
AIM- Motion Coherence HC	283 ±126	216 ±83	94 ±42	72 ±28
FInD- Form Coherence	263 ±288	182 ±124	29 ±32	20 ±14
FInD- Form Coherence HC	365 ±332	225 ±140	40 ±37	25 ±16
FInD- Form Coherence	306 ±165	248 ±99	34 ±18	28 ±11
FInD- Form Coherence HC)	360 ±139	301 ±149	40 ±15	33 ±17

Exploratory Correlation and Cluster Analysis

After assessing the test's repeatability and gaining insights into the normative range of performance within each test, we explored how these performance results relate to one another. Hence, we conducted a linear regression and hierarchical cluster analysis to investigate the relationship between outcome parameters. Kendall's correlation coefficients between all tests were calculated. The matrix in Figure 3 shows the correlation coefficients between all tests as color-code and value in each cell of the matrix. The warmer colors indicate higher and the colder colours lower correlations (see colour bar). The asterisks indicate whether the correlation was significantly different from zero. This analysis reveals significant correlations within CSF and between motion coherence outcomes but few significant correlations between form coherence outcomes. The marginal cluster trees in Figure 3 show results from a hierarchical cluster analysis using Ward's Minimum Variance Clustering Method based on the Euclidean distance between objects (i.e., tests).

This analysis revealed overall clustering of CSF, Form and Motion tests.

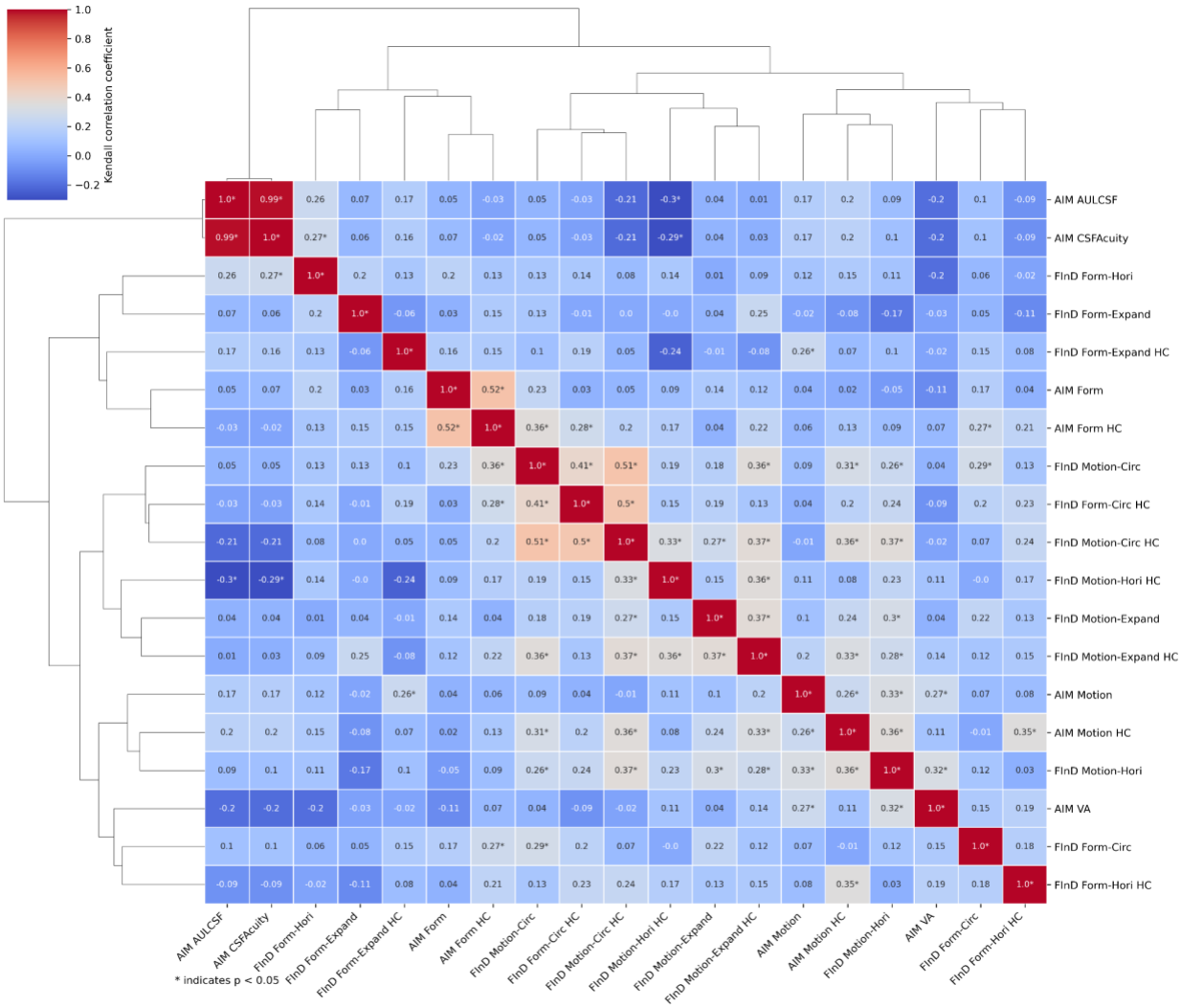

Figure 3 (i) The figure shows Kendall's correlation coefficients between all tests as color-code and value in each cell of the matrix, where warmer colors indicate higher correlations (see color bar). The asterisks indicate whether the correlation was significantly different from zero. (ii) The marginal cluster trees show results from a hierarchical cluster analysis). Note that the data set includes a dependent set of CSF Acuity and AULCSF data that is derived from the same logparabola fit function in each observer.

Correlation between performance and ASRS and AQ scores

In future work, we aim to investigate whether performance is affected by Asperger syndrome (i.e., high-functioning autism) or attention deficit hyperactivity disorder (ADHD). Here, we examine normative performance in a neurotypical population of young adults, therefore, all subjects filled out the Adult ADHD Self-Report Scale (ASRS, Kessler *et al.*, 2005) and the autism-spectrum quotient (AQ, Baron-Cohen *et al.*, 2001) questionnaires. The results from these questionnaires are summarized in Table 1. We subsequently calculated Pearson's linear correlation coefficients between all tests and the ASRS and AQ scores. The correlation plots, including the

correlation coefficients and p-values are shown in the supplementary ASRS_AQ_correlations.pdf. None of these correlations was significant in our neurotypical population.

Discussion

The first goal of this study was to investigate the repeatability of the AIM and FInD paradigms in neurotypical healthy young adults for a variety of visual functions (acuity, contrast sensitivity, form- and motion coherence) performed on a tablet computer.

Comparison with previous FInD and AIM studies

AIM Visual Acuity: Previous studies investigated the repeatability of AIM VA for a viewing distance of 4m instead of near testing as performed in the current study (Skerswetat *et al*., 2024a). That study showed that increasing the number of adaptive charts reduces the repeatability variance as expressed using limits of agreement which for 3 charts i.e., one initial and two adaptive steps ±0.24 logMAR was comparable to the ±0.14 logMAR (CoR: ±0.19 logMAR) of the current study. Also, the current study and the previous study found no systematic retest bias.

Form and Motion: A study in patients with and without cerebral visual impairment (Merabet *et al*., 2023) reported 27% for circular motion and 30% for form thresholds using the hidden cell FInD tasks in the control cohort, which is slightly different to 18% and 39%, respectively, as reported in the current study's first test session (Table 2). This may be due to the different stimulus properties of the tablet used here and the 32" computer display used in Merabet *et al.* (2023). We are not aware of any published estimates of test-retest repeatability of coherence measured with other paradigms, such as 2AFC. In a study concerning vision in people with and without albinism (Skerswetat *et al.*, 2024b), thresholds for the control group, using FInD circular Motion and Form Coherence with hidden cells mode, were 22% and 52%, respectively. Again, higher sensitivity in motion compared to form coherence was shown, but lower sensitivity for form coherence, which can be explained due to the higher age of the cohort since form coherence thresholds increase with age (McKendrick, Weymouth & Battista, 2013). FInD complex motion and form coherence tasks showed no significant mean biases, whereas bias was found here for translation, simple form and motion signals (Table 2). Future research may investigate whether the bias reflects learning and might disappear between a second and third session. In the meantime, it is suggested to run an initial training session prior to an actual task for these stimulus types. The study also revealed a wide inter-individual difference in the ability to perceive global motion and form (Figure 3).

AIM CSF 2D + showed no retest bias but had significantly larger variance when using three charts compared to five charts. Hence, it is suggested to use five charts as default to ensure minimum retest variance.

Psychometric parameters

Some previous studies have investigated slope parameters (e.g., Wallis *et al.*, 2013), however to our best knowledge no study specifically looked at the repeatability of slope parameters. Table 3 shows the slope and table 4 the minimum report error or *noise* (i.e., result of all noise factors) with the corresponding repeatability results. With the exception of CSF results using three charts, all slopes were bias free. The noise parameters were mostly bias-free except for FInD Form circular coherence and hidden cell expanding coherence. These results show that the methods employed in the AIM and FInd paradigms produce consistent and repeatable measurements.

Testing durations

The average time for visual acuity (Table 5) was less than two minutes in total and an approximate chart duration of 30 seconds, which is comparable to previously reported times when testing for distance visual acuity (Skerswetat *et al.*, 2024a). The mean chart duration was less than one minute for the CSF task, hence the total duration for 5 charts is approximately 4 minutes, which is faster than conventional tests that may take 25 minutes (Kelly & Savoie, 1973) and comparable to other adaptive rapid procedures (Liu *et al*., 2021).

The test durations for the Form and Motion tasks varied more widely specifically between 3 and 6 minutes per tests, one because the FInD task tested three subtypes of form and motion percepts, namely horizontal, circular and expanding percepts, compared to translational, simple form or motion percepts. The hidden cell paradigms caused longer testing durations than the open cell paradigms. This may be due to either the use of a mouse instead of finger touches, different gaze strategies used to detect signals, or a combination of those reasons. Since we did not collect gaze position data, future studies may investigate whether different gaze strategies were used for open and hidden cell modes.

Functional relationship between psychometric outcomes

The second goal of the study was to investigate relationships among thresholds. We used a combination of linear models and hierarchical cluster analysis, unlike in a previous study where these analyses were performed separately (Skerswetat *et al*., 2024b). The current study shows overall within-function outcomes clustering, specifically for contrast - contrast, form - form, and motion - motion outcomes (Figure 2). Similarly, contrast outcomes correlated with each other, as well as motion outcomes. Skerswetat *et al.* (2024b) and Bosten *et al.* (2017) also found significant correlations among contrast outcomes, but not among motion values. We speculate

that this difference may be due to the more heterogeneous age range and smaller sample within the control cohort of that study compared to the current study. The same study (Skerswetat *et al.*, 2024b) also showed clustering within contrast and within form and motion outcomes for the control cohort, which is in agreement with the current study. Overall, these results suggest distinct processing pathways of contrast and mid-level form and motion perception.

Although the primary aim of this study was to assess the repeatability of the tests, the results—particularly those obtained from the AIM and FInD Form and Motion tests—also provide insight into the visual processing of global texture and motion. A detailed analysis, along with further discussion and comparisons with previous studies, is presented in the Appendix and Figure A2.

Future directions

The current study investigated the repeatability and functional relationship of the tablet-based psychophysical tests in young healthy participants. Based on the high repeatability of these results and the normative data, future research can be adequately powered to test the effect of age and the effect in clinically relevant cohorts on the test performance. The number of cells within each chart and the number of charts determine the testing duration, and the present data can guide future research to investigate their relationship to optimise the time-repeatability tradeoff.

Conclusion

AIM and FInD near vision tests are generalizable across multiple visual functions and are precise and reliable. Most functions tested were bias-free, except translational form and motion coherence, which showed significant improvement on a second test. In future studies, such bias may be improved with additional instructions or training charts. CSF, form, and motion outcomes clustered together, and CSF and motion outcomes correlated with one another, indicating separate processing mechanisms for achromatic spatial and global coherence perception. Together, the results demonstrate the reliability of the tests, which may be useful for basic and clinical research.

Acknowledgements

Conflict of interest: JS and PJB are co-founders and shareholders of PerZeption Inc. JS and PJB are the inventors of AIM and FInD technology (P). Northeastern University is the owner of the intellectual property and granted exclusive licensing rights to PerZeption Inc.

GS and JG were supported by the College of Optometrists (UK).

PJB and JS were supported by NIH R01EY032162.

References

Achtman, R., Hess, R. F., & Wang, Y. Z. (2003). Sensitivity for global shape detection. Journal of Vision, 3(10):4, 616–624 https://doi.org/10.1167/3.10.4

Ahmed Z., Skerswetat J., Bex P.J. & Wiecek E.K. (2023). Assessment of Visual Acuity in Children With and Without Amblyopia Using the Novel Method AIM (Angular Indication Measurement) Acuity. Investigative Ophthalmology & Vision Science 2023;64(8):1505 Available at: https://iovs.arvojournals.org/article.aspx?articleid=2790964

Allard, R., Faubert, J. (2008)The noisy-bit method for digital displays: Converting a 256 luminance resolution into a continuous resolution. *Behavior Research Methods* 40, 735–743. https://doi.org/10.3758/BRM.40.3.735

Altman, D. G., & Bland, J. M. (1983). Measurement in medicine: the analysis of method comparison studies. Journal of the Royal Statistical Society Series D: The Statistician, *32*(3), 307-317.http://dx.doi.org/10.2307/2987937

Arthur, C., He, J., Bex, P., Skerswetat, J. & Crognale, M. (2025) Application of the angular indication measurement and foraging interactive D-prime paradigms to tablet-based color vision testing. Journal of the Optical Society of America A: Optics and Image Science, and Vision, 42(5):B432-B442. http://doi.org/10.1364/JOSAA.545286

Baron-Cohen, S., Wheelwright, S., Skinner, R., Martin, J., & Clubley, E. (2001). The autism-spectrum quotient (AQ): Evidence from asperger syndrome/high-functioning autism, males and females, scientists and mathematicians. Journal of autism and developmental disorders, 31, 5-17.

Bano, T., Wolffsohn, J.S. & Sheppard, A.L. (2024) Assessment of visual function using mobile Apps. Eye 38:2406–2414 https://doi.org/10.1038/s41433-024-03031-2

Bex P. & Skerswetat J. (2021) FInD - Foraging Interactive D-prime, a rapid and easy general method for visual function measurement. Journal of Vision 21(9):2817 https://doi.org/10.1167/jov.21.9.2817

Bex P.J. & Skerswetat J. (2023) AIM+ (Angular Indication Measurement) Efficient Assessment of Multidimensional Functions;45th European Conference on Visual Perception (ECVP) 2023 Paphos, Cyprus Perception (Collections: ECVP Abstracts) pp202-3. Available at: https://journals.sagepub.com/page/pec/collections/ecvp-abstracts/index/ecvp-2023

Bosten, J., Goodbourn, P. T., Bargary, G., Verhallen, R. J., Lawrance-Owen, A. J., Hogg, R. E., & Mollon, J. D. (2017a). An exploratory factor analysis of visual performance in a large population. Vision Research, 141, 303-316. https://doi.org/10.1016/j.visres.2017.02.005

Bosten, J., Mollon, J., Peterzell, D. & Webster, M. (2017b) Individual differences as a window into the structure and function of the visual system. Vision Research, 141, 1-3. https://doi.org/10.1016/j.visres.2017.11.003

Bourne, R. and GBD 2019 Blindness and Vision Impairment Collaborators (2021) Trends in prevalence of blindness and distance and near vision impairment over 30 years: an analysis for the Global Burden of Disease Study. The Lancet Global Health 9(2):e130 - e143 https://doi.org/10.1016/S2214-109X(20)30425-3

Braddick, O. J., O'Brien, J. M., Wattam-Bell, J., Atkinson, J., & Turner, R. (2000). Form and motion coherence activate independent, but not dorsal/ventral segregated, networks in the human brain. Current Biology, 10(12), 731–734 https://doi.org/10.1016/s0960-9822(00)00540-6

Britten, K.H. & Newsome, W.T. (1998) Tuning Bandwidths for Near-Threshold Stimuli in Area MT. Journal of Neurophysiology 80:2, 762-770 https://doi.org/10.1152/jn.1998.80.2.762

Cadieu, C., Kouh, M., Pasupathy, A., Connor, C. E., Riesenhuber, M., Poggio, T., & Pasupathy, A. (2007). A model of V4 shape selectivity and invariance. Journal of Neurophysiology, 98(3), 1733–1750 https://doi.org/10.1152/jn.01265.2006

Cappe, C., Clarke, A., Mohr, C. & Herzog, M. (2014) Is there a common factor for vision? Journal of Vision, 14(8), 4. https://doi.org/10.1167/14.8.4

Chen, C., Ding, S. & Wang, J. (2023) Digital health for aging populations. Nature Medicine 29:1623–1630 https://doi.org/10.1038/s41591-023-02391-8

Cumberland PM, Rahi JS, for the UK Biobank Eye and Vision Consortium (2016) Visual Function, Social Position, and Health and Life Chances: The UK Biobank Study. JAMA Ophthalmology 134(9):959–966 https://doi:10.1001/jamaophthalmol.2016.1778

Dakin, S. C., & Bex, P. J. (2002). Summation of concentric orientation structure: Seeing the Glass or the window? Vision Research, 42(16), 2013–2020 https://doi.org/10.1016/S0042-6989(02)00057-3

Dakin, S. C. (1997). The detection of structure in glass patterns: Psychophysics and computational models. Vision Research, 37(16), 2227–2246 https://doi.org/10.1016/S0042-6989(97)00038-2

Dickinson, J.E., Broderick C., Badcock D.R. (2009) Selective attention contributes to global processing in vision. Journal of Vision 9(2):6 https://doi.org/10.1167/9.2.6

Elam, A. R., Tseng V. L., Rodriguez T. M., Mike E. V., Warren A. K., Coleman A. L. and American Academy of Ophthalmology Taskforce on Disparities in Eye Care (2022) Disparities in Vision Health and Eye Care. Ophthalmology 129 (10):e89-e113 https://doi.org/10.1016/j.ophtha.2022.07.010

Garobbio, S., Kunchulia, M. & Herzog, M. (2024) Weak correlations between visual abilities in healthy older adults, despite long-term performance stability. Vision Research, 215, 108355. https://doi.org/10.1016/j.visres.2023.108355

Glass, L., & Perez, R. (1973). Perception of random dot interference patterns. Nature, 246, 360–362 https://doi.org/10.1038/246360a0

Glass, L. (1969). Moiré effect from random dots. Nature, 223, 578–580 https://doi.org/10.1038/223578a0

He J., Bex P.J. & Skerswetat J. (2023) Rapid measurement and machine learning classification of colour vision deficiency. Ophthalmic and Physiological Optics 43:1379–1390 https://doi.org/10.1111/opo.13210

He J., Skerswetat J. & Bex P.J. (2023) Novel color vision assessment tools: AIM Color Detection and Discrimination. Investigative Ophthalmology & Visual Science, 64(8), 1509. https://iovs.arvojournals.org/article.aspx?articleid=2791073

Herzog, M., Garobbio, S., Pfau, M. & Scholl, H. (2025) Is there a common factor for vision? Acta Ophthalmologica, 103, S284. https://doi.org/10.1111/aos.16974

Kelly, D. M., Bischof, W. F., Wong-Wylie, D. R., & Spetch, M. L. (2001). Detection of glass patterns by pigeons and humans: Implications for differences in higher-level processing. Psychological Science, 12(4), 338–342. https://doi.org/10.1111/1467-9280.00362

Kelly D. H., Savoie R. E. (1973). A study of sine-wave contrast sensitivity by two psychophysical methods. Perception & Psychophysics, 14, 313–318. https://doi.org/10.3758/BF03212397

Kessler, R., Adler, L., Ames, M., Demler, O., Faraone, S., Hiripi, E., Howes, M., Jin, R., Secnik, K., Spencer, T., Bedirhan Ustun, T. & Walters, E. (2005). The World Health Organization Adult ADHD Self-Report Scale (ASRS): a short screening scale for use in the general population. Psychological medicine, 35(2), 245-256. https://doi:10.1017/S0033291704002892

Khurana R. N., Hoang C., Khanani A. M., Steklov N. & Singerman L. J. (2021) A Smart Mobile Application to Monitor Visual Function in Diabetic Retinopathy and

Age-Related Macular Degeneration: The CLEAR Study. American Journal of Ophthalmology 227:222-230 https://doi.org/10.1016/j.ajo.2021.03.033

Killeen OJ, De Lott LB, Zhou Y, Hu M., Rein D., Reed N., Swenor B.K. & Ehrlich J.R. (2023) Population Prevalence of Vision Impairment in US Adults 71 Years and Older: The National Health and Aging Trends Study. JAMA Ophthalmology 141(2):197–204 https://doi:10.1001/jamaophthalmol.2022.5840

Kurki, I., & Saarinen, J. (2004). Shape perception in human vision: Specialized detectors for concentric spatial structures? Neuroscience Letters, 360(1-2), 100–102 https://doi.or/10.1016/j.neulet.2004.01.053

Liu J., Bex P.J., Jnawali A. & Vera-Diaz F.A. (2021) Evaluation of the novel Foraging Interactive D-prime (FInD) CSF Test. Investigative Ophthalmology & Vision Science 62(8):525. Available at: https://iovs.arvojournals.org/article.aspx?articleid=2774587

Martínez-roda, J. A., Vilaseca, M., Ondategui, J. C., Aguirre, M., & Pujol, J. (2016) Effects of aging on optical quality and visual function. Clinical and Experimental Optometry 99(6):518–525. https://doi.org/10.1111/cxo.12369

McKendrick, A.M., Weymouth, A.E. & Battista, J. (2013) Visual Perception from Age 20 through 80 Years. Investigative Ophthalmology & Visual Science 54(3):1730-1739 https://10.1167/iovs.12-10974

Merabet L.B., Manley C.E., Pamir Z., Bauer C.M., Skerswetat J. & Bex P.J. (2023) Motion and form coherence processing in individuals with cerebral visual impairment. Developmental Medicine & Child Neurology 65:1379–1386. https://doi.org/10.1111/dmcn.15591

Neupane S., Skerswetat J. & Bex P.J. (2024) Comparison of Foraging Interactive D-prime and Angular Indication Measurement Stereo with different methods to assess stereopsis. PLOS ONE 19(6):e0305036. https://doi.org/10.1371/journal.pone.0305036

Newsome, W. T., & Pare, E. B. (1988). A selective impairment of motion perception following lesions of the middle temporal visual area (MT). Journal of Neuroscience, 8(6), 2201-2211. https://doi.org/10.1523/JNEUROSCI.08-06-02201.1988

Pei, F., Pettet, M. W., Vildavski, V. Y., & Norcia, A. M. (2005). Event-related potentials show configural specificity of global form processing. NeuroReport, 16(13), 1427–1430. https://doi.org/10.1097/01.wnr.0000177003.12322.9b

Rasdall M.A., Cho C., Stahl A.N., Tovar D.A., Lavin P., Kerley C.I., Chen Q., Ji X., Colyer M.H., Groves L., Longmuir R., Chomsky A., Gallagher M.J., Anderson A., Landman B.A. & Rex T.S. (2024) Primary Visual Pathway Changes in Individuals

With Chronic Mild Traumatic Brain Injury. JAMA Ophthalmology https://doi:10.1001/jamaophthalmol.2024.5076

Rizzo, J. R., Beheshti, M., Hudson, T. E., Mongkolwat, P., Riewpaiboon, W., Seiple, W., Ogedegbe O.G. & Vedanthan, R. (2020) The global crisis of visual impairment: an emerging global health priority requiring urgent action. Disability and Rehabilitation: Assistive Technology, 18(3):240–245. https://doi.org/10.1080/17483107.2020.1854876

Samanta A, Mauntana S, Barsi Z, Yarlagadda B, Nelson PC. (2023) Is your vision blurry? A systematic review of home-based visual acuity for telemedicine. Journal of Telemedicine and Telecare 29(2):81-90 https://doi:10.1177/1357633X20970398

Schmidtmann, G., Gordon, G. E., Bennett, D. M., & Loffler, G. (2013). Detecting shapes in noise: tuning characteristics of global shape mechanisms. Frontiers in Computational Neuroscience, 7(37), 1–14 https://doi.org/10.3389/fncom.2013.00037

Schmidtmann, G., Jennings, B. J., Bell, J., Kingdom, F.A.A. (2015). Probability, not linear summation, mediates the detection of concentric orientation-defined textures. *Journal of Vision*, *15*(16), 1-19 https://doi.org:10.1167/15.16.6

Serre, T., Kouh, M., Cadieu, C., Knoblich, U., Kreiman, G. & Poggio, T. (2005). A theory of object recognition: computations and circuits in the feedforward path of the ventral stream in primate visual cortex. AI Memo 2005–036/CBCL Memo 259. Cambridge, MA: MIT. Available at: http://hdl.handle.net/1721.1/36407

Serre, T., Oliva, A., & Poggio, T. (2007). A feedforward architecture accounts for rapid categorization. Proceedings of the National Academy of Sciences, USA, 104(15), 6424–6429 https://doi.org:10.1073/pnas.0700622104

Seu, L., & Ferrera, V. P. (2001). Detection thresholds for spiral Glass patterns. Vision Research, 41(28), 3785–3790 https://doi.or/10.1016/s0042-6989(01)00235-8

Shaqiri, A., Pilz, K., Cretenoud, A., Neumann, K., Clarke, A., Kunchulia, M. & Herzog, M. (2019) No evidence for a common factor underlying visual abilities in healthy older people. Developmental Psychology, 55(8), 1775-1787. https://doi.org/10.1037/dev0000740

Skerswetat J. & Bex P.J. (2022) AIM+(Angular Indication Measurement Plus) enables rapid and self-administered assessment of visual perception dependency across multiple stimulus dimensions; 44th European Conference on Visual Perception (ECVP) 2022 Nijmegen, The Netherlands, Perception 51(1_Suppl):34 https://doi.org/10.1177/03010066221141167

Skerswetat J., Boruta A. & Bex P.J. (2022) Disability Glare Quantified Rapidly with AIM (Angular Indication Measurement) Glare Acuity. Investigative Ophthalmology & Vision Science 63(7):2558 – F0512 Available at: https://iovs.arvojournals.org/article.aspx?articleid=2783354

Skerswetat J., He J., Shah J.B., Aycardi N., Freeman M. & Bex P.J. (2024a) A new, adaptive, self-administered, and generalizable method used to measure visual acuity Optometry and Vision Science 101:451–463 https://doi.org/10.1097/OPX.0000000000002160

Skerswetat J., Ross N.C., Idman-Rait C., Sun K., Wynn O. & Bex P.J. (2024b) Visual Performance of People With Albinism Assessed With Generalizable and Adaptive AIM and FInD Methods. Investigative Ophthalmology & Visual Science 65(11):34 https://doi.org/10.1167/iovs.65.11.34

Smith, M. A., Bair, W., & Movshon, J. A. (2002). Signals in macaque striate cortical neurons that support the perception of glass patterns. Journal of Neuroscience, 22(18), 8334–8345 https://doi.org/10.1523/JNEUROSCI.22-18-08334.2002

Smith, M. A., Kohn, A., Movshon, J. A., & Movshon, J. A. (2007). Glass pattern responses in macaque V2 neurons. Journal of Vision, 7(3):5, 1–15 Available at: https://doi.org/10.1167/7.3.5

Tulver, K. (2019) The factorial structure of individual differences in visual perception. Consciousness and Cognition, 73, 102762. https://doi.org/10.1016/j.concog.2019.102762

United Nations (2022) World Population Prospects 2022: Summary of Results. United Nations. Available at: https://www.un.org/development/desa/pd/sites/www.un.org.development.desa.pd/files/wpp2022_summary_of_results.pdf

Van Essen, D., Anderson, C., & Felleman, D. (1992). Information processing in the primate visual system: An integrated systems perspective. Science, 255(5043), 419–423 https://doi.or/10.1126/science.1734518

Wallis, S. A., Baker, D. H., Meese, T. S., & Georgeson, M. A. (2013). The slope of the psychometric function and non-stationarity of thresholds in spatiotemporal contrast vision. *Vision research*, *76*, 1-10. https://doi.org/10.1016/j.visres.2012.09.019

Walter K, Bex P (2024) A novel, rapid, quantitative method for face discrimination. PLOS ONE 19(12): e0315998 https://doi.org/10.1371/journal.pone.0315998

Waskom, M. L., (2021). seaborn: statistical data visualization. Journal of Open Source Software, 6(60), 3021, https://doi.org/10.21105/joss.03021

Watson, A. B., & Ahumada, A. J. (2005). A standard model for foveal detection of spatial contrast. *Journal of vision*, *5*(9), 717-740. https://doi.org/10.1167/5.9.6

Wilson, H., Wilkinson, F., (1998) Detection of global structure in Glass patterns: Implications for form vision. Vision Research, 38, 2933–2947 https://doi.or/10.1016/S0042-6989(98)00109-6

Wilson, H., Wilkinson, F., & Asaad, W. (1997). Concentric orientation summation in human form vision. Vision Research, 37(17), 2325–2330 https://doi.org/10.1016/s0042-6989(97)00104-1

World Health Organisation (2019) World report on vision. World Health Organisation. Available at: https://www.who.int/publications/i/item/world-report-on-vision

World Health Organisation (2022) Report of the 2030 targets on effective coverage of eye care. Available at: https://www.who.int/publications/i/item/9789240058002

World Health Organization (2023) Increasing eye care interventions to address vision impairment: Technical Brief. World Health Organization. Available at: https://www.who.int/publications/m/item/increasing-eye-care-interventions-to-address-vision-impairment

868 **Appendix**

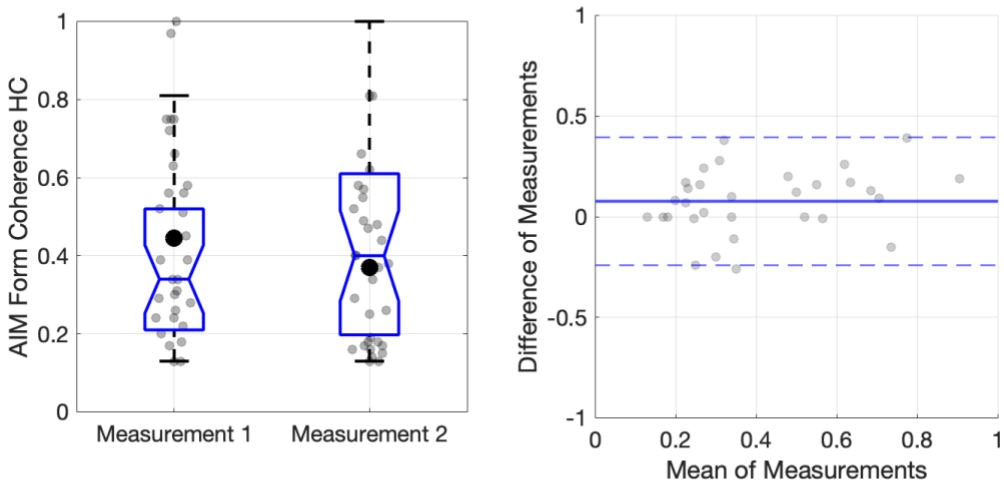

869

870 **Figure A1** Left: Example data showing Box and Whisker plots with individual data (grey data points)
871 and the mean (black solid data point) for the AIM Form Coherence test (coherence thresholds are
872 expressed in %, 0-1). Right: Bland-Altman plots for AIM Form Coherence. Figures for all tests can be
873 found in the supplementary material (Bland_Altman_plots.pdf).

874

875 **Comparison between horizontal, expanding and circular form and motion**

876 The results from the AIM and FInD Form and Motion tests have implications
877 regarding the visual processing of global texture and motion. There is ample
878 psychophysical and physiological evidence for the hypothesis that the representation
879 of objects and shapes is achieved by a hierarchical feedforward process along the
880 ventral pathway (e.g., Cadieu *et al*., 2007; Serre *et al.*, 2005; Serre, Oliva, & Poggio,
881 2007; Van Essen, Anderson, & Felleman, 1992). A key question in vision science is
882 how local information detected in the early visual areas (primary visual cortex) is
883 integrated to represent more complex, behaviorally relevant stimuli (e.g., faces,
884 objects) at subsequent stages. Psychophysically, this has been tested in different
885 ways. One approach, also employed in the Form and Motion tests, is to determine
886 the minimum number of signal elements required to detect the presence of a global
887 pattern embedded in an array of noise elements (coherence thresholds). This

measurement of coherence thresholds has been used in many studies of motion (Braddick *et al*., 2000; Newsome, 1988), texture (Dakin, 1997; Schmidtmann *et al*., 2015; Wilson & Wilkinson, 1998; Wilson, Wilkinson, & Asaad, 1997), and contour perception (Achtman, Hess, & Wang, 2003; Braddick *et al*., 2000; Schmidtmann *et al*., 2013; 2015). Coherence thresholds in Glass patterns (Glass, 1969; Glass & Perez, 1973) have been employed to investigate signal integration in texture perception (Dakin, 1997; Dakin & Bex, 2002; Dickinson, Broderick, & Badcock, 2009; Wilson, Wilkinson & Asaad, 1997; Wilson & Wilkinson, 1998). Models of Glass pattern detection propose a two-stage process, in which the first stage extracts local orientation information while the second stage integrates the orientation information in order to extract the global structure (Wilson, Wilkinson & Assad, 1997; Wilson & Wilkinson, 1998, see Schmidtmann *et al.* (2015) for a revised model). This model is supported by physiological data showing that neither the classical receptive fields nor surround mechanisms in early visual areas (V1, V2) are sufficient to process the Glass patterns (Smith, Bair, & Movshon, 2002; Smith *et al*., 2007). Some previous psychophysical studies found no difference in sensitivities for detecting circular and radial structure (e.g., see Kelly *et al.*, 2001; Kurki & Saarinen, 2004; Pei *et al.*, 2005; Seu & Ferrera, 2001; Wilson, Wilkinson & Asaad, 1997; Wilson & Wilkinson, 1998), while others reported a significantly increased sensitivity of human observers for circular, followed by radial, spiral, and parallel structure (Kelly *et al.*, 2001; Kurki & Saarinen, 2004; Seu & Ferrera, 2001; Wilson, Wilkinson & Asaad, 1997; Wilson & Wilkinson, 1998), suggesting that the global structure in Glass patterns is processed by specialized detectors for circular and radial textures. However, there is also contradictory evidence. For instance, Dakin and Bex (2002) found that the advantage for circular Glass patterns was only evident if the stimulus was presented within a circular window as opposed to a square window. Similarly, Schmidtmann *et al.* (2015) were not able to replicate the above mentioned hierarchy. Their results showed that detection sensitivity was independent of texture type; hence, no evidence for specialized detectors for circular structure.

The results presented here also do not show the clear sensitivity hierarchy (i.e., circular > expanding > horizontal) described above. Figure A2 shows Box and Whisker plots comparing coherence thresholds achieved for horizontal, expanding and circular structure for the FInD Form, FInD Form HC, FInD Motion, and FInD Motion HC tests. Following Shapiro-Wilk tests for normality, which showed that some of the conditions were not normally distributed, the data were analyzed using a non-parametric Friedman ANOVA (Durbin-Conover) across all conditions. This analysis revealed a statistically significant global effect ($\chi^2(119) = 11$, $p<.001$). Subsequent pairwise comparisons (Bonferroni-corrected for multiple comparisons) showed that for the FInD Form paradigms, sensitivity was largely independent of texture type, except for a statistically significant increase in thresholds (i.e. decrease in sensitivity) between FInD Form HC horizontal and FInD Form HC circular. In general, performance for the FInD Motion paradigms was slightly (sometimes significantly better; see Table A1) compared to the static FInD Form stimuli. Results show that sensitivity for FInD Motion horizontal and FInD Motion expanding stimuli was

significantly lower compared to FInD Motion circular. Finally, sensitivity for FInD Motion HC expanding was significantly lower compared to FInD Motion HC circular and FInD Motion HC horizontal. No superior performance for circular motion is evident.

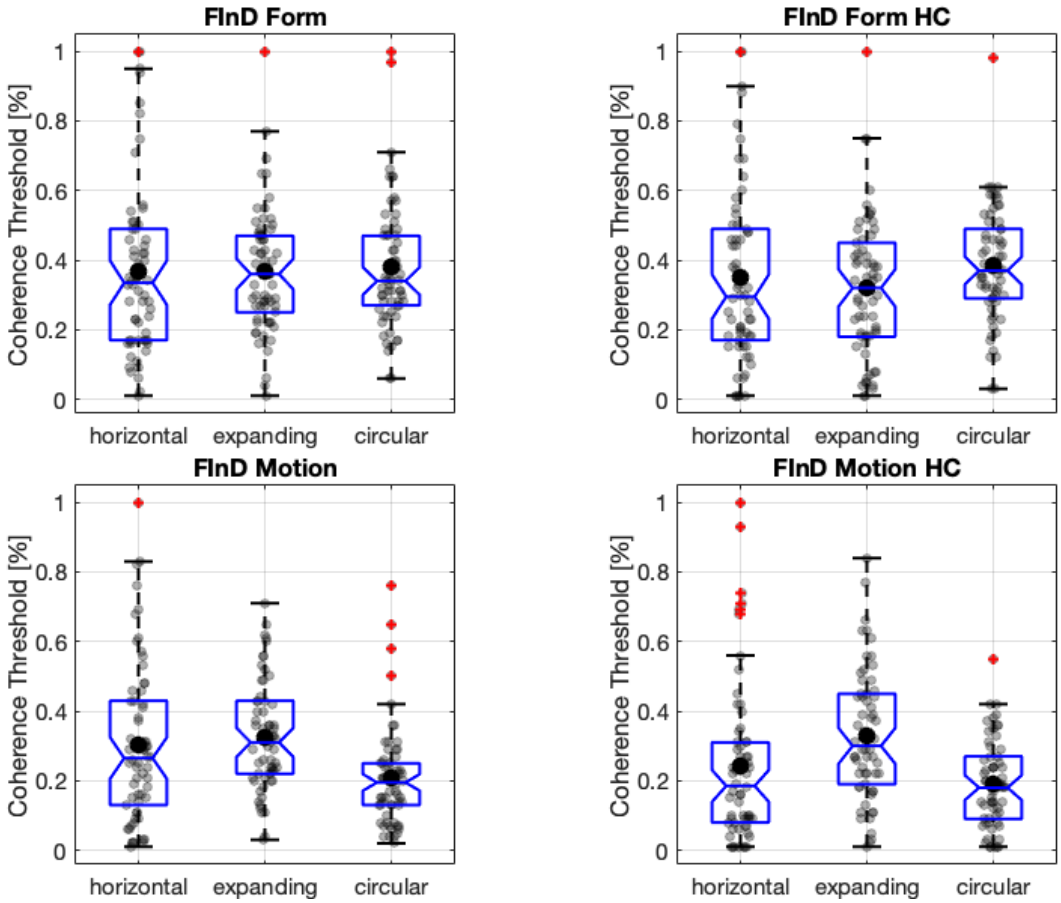

Figure A2 Box and Whisker plots with individual data (grey data points) and the mean (black solid data point) for the FInD Form (top left), FInD Form HC (top right), FInD Motion (bottom left) and FInD Motion HC (bottom right) tests (coherence thresholds are expressed in %, 0-1). The outliers (red diamonds) with coherence thresholds of ~1 (~100%) were from two subjects who could not do the task, independent of global structure.

‘

Table A1 non-parametric Friedman ANOVA pairwise comparison (Durbin-Conover). Statistically significant conditions are indicated by *.

Pairwise Comparisons (Durbin-Conover)		Statistic	*p*
FInD Form circ	FInD Motion HC circ	7.0448	< .001*
FInD Form HC hori	FInD Form HC exp	0.218	0.827
FInD Form HC hori	FInD Form HC circ	2.8615	0.004*
FInD Form HC hori	FInD Motion hori	0.1635	0.87
FInD Form HC hori	FInD Motion exp	1.022	0.307
FInD Form HC hori	FInD Motion circ	4.2923	< .001*
FInD Form HC hori	FInD Motion HC hori	3.2431	0.001*
FInD Form HC hori	FInD Motion HC exp	1.4308	0.153
FInD Form HC hori	FInD Motion HC circ	4.5784	< .001*
FInD Form HC exp	FInD Form HC circ	2.6435	0.008*
FInD Form HC exp	FInD Motion hori	0.3815	0.703
FInD Form HC exp	FInD Motion exp	0.804	0.422
FInD Form HC exp	FInD Motion circ	4.5103	< .001*
FInD Form HC exp	FInD Motion HC hori	3.4611	< .001*
FInD Form HC exp	FInD Motion HC exp	1.2127	0.226
FInD Form HC exp	FInD Motion HC circ	4.7965	< .001*
FInD Form HC circ	FInD Motion hori	3.025	0.003*
FInD Form HC circ	FInD Motion exp	1.8396	0.066
FInD Form HC circ	FInD Motion circ	7.1538	< .001*
FInD Form HC circ	FInD Motion HC hori	6.1046	< .001*
FInD Form HC circ	FInD Motion HC exp	1.4308	0.153
FInD Form HC circ	FInD Motion HC circ	7.44	< .001*
FInD Motion hori	FInD Motion exp	1.1855	0.236
FInD Motion hori	FInD Motion circ	4.1288	< .001*
FInD Motion hori	FInD Motion HC hori	3.0795	0.002*
FInD Motion hori	FInD Motion HC exp	1.5943	0.111
FInD Motion hori	FInD Motion HC circ	4.4149	< .001*
FInD Motion exp	FInD Motion circ	5.3143	< .001*
FInD Motion exp	FInD Motion HC hori	4.265	< .001*
FInD Motion exp	FInD Motion HC exp	0.4088	0.683
FInD Motion exp	FInD Motion HC circ	5.6004	< .001*
FInD Motion circ	FInD Motion HC hori	1.0492	0.294
FInD Motion circ	FInD Motion HC exp	5.7231	< .001*
FInD Motion circ	FInD Motion HC circ	0.2862	0.775
FInD Motion HC hori	FInD Motion HC exp	4.6738	< .001*
FInD Motion HC hori	FInD Motion HC circ	1.3354	0.182
FInD Motion HC exp	FInD Motion HC circ	6.0092	< .001*

Contrast Sensitivity Function

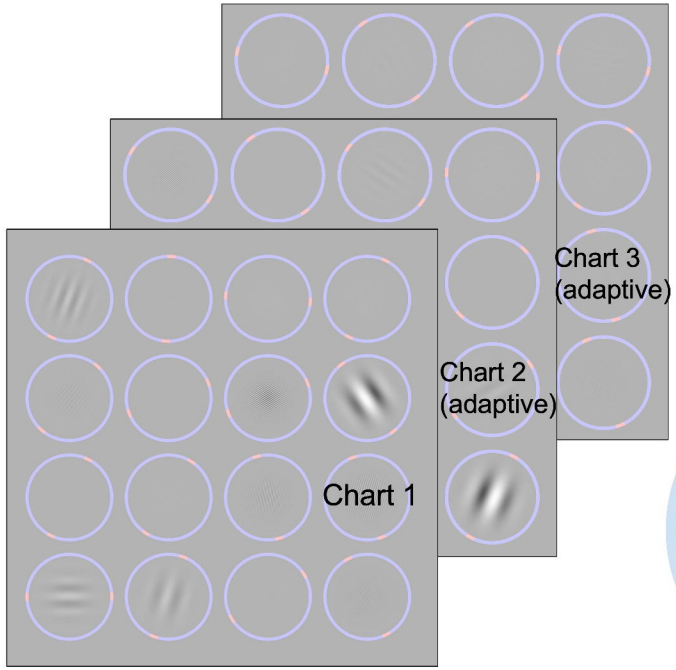

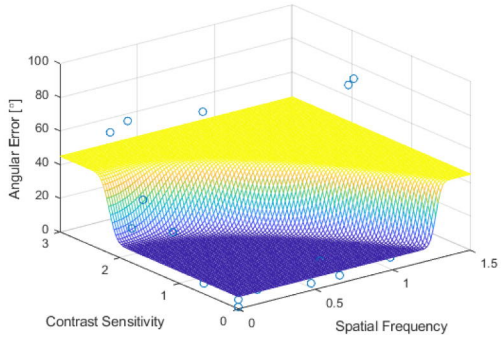

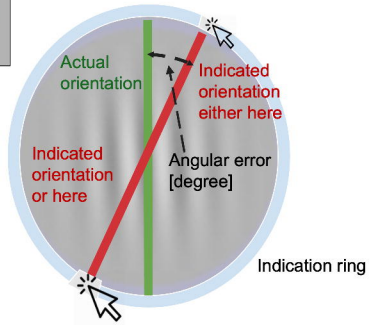

Form Coherence

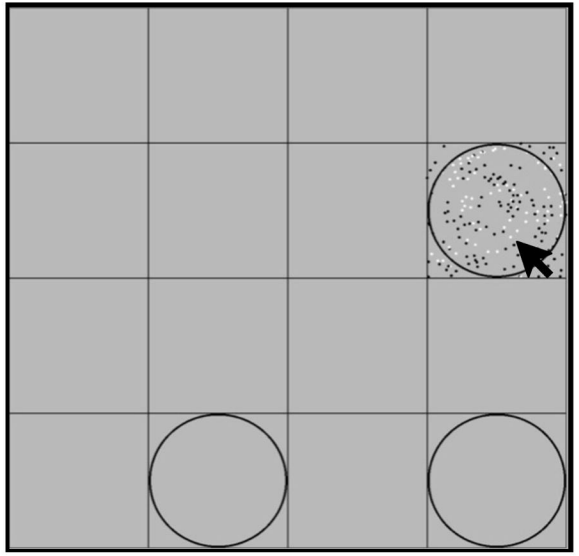

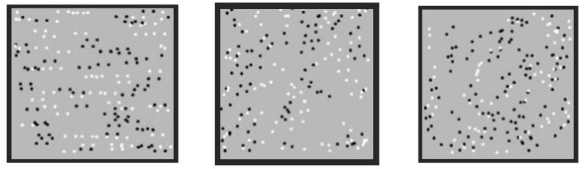

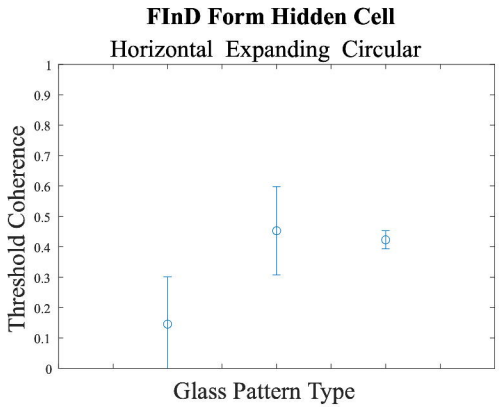

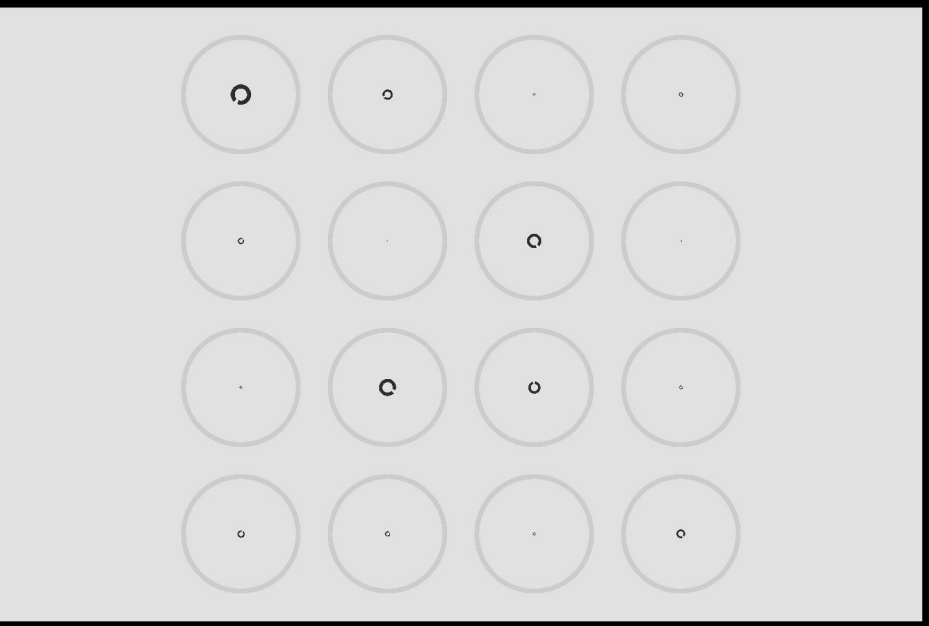

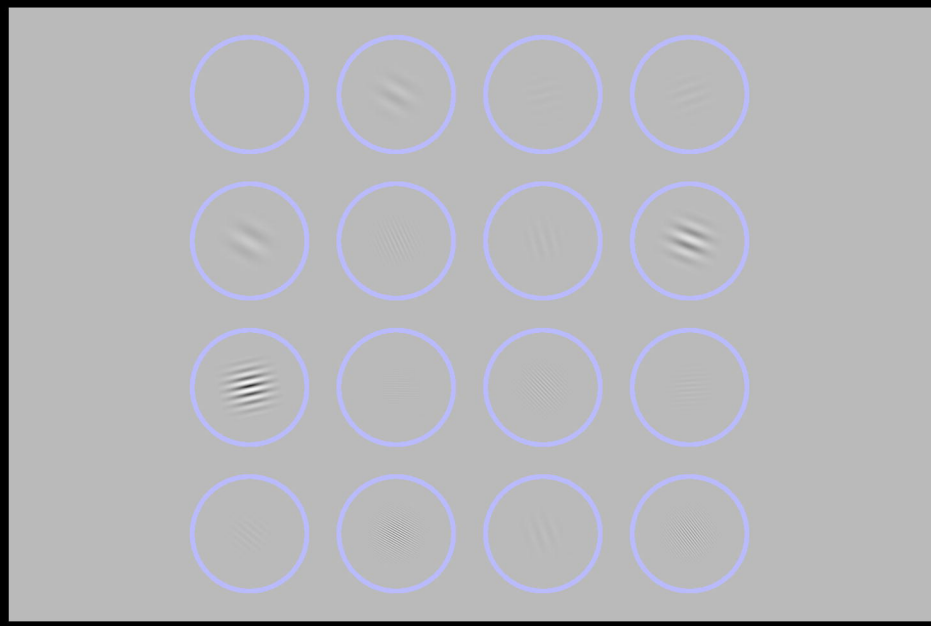

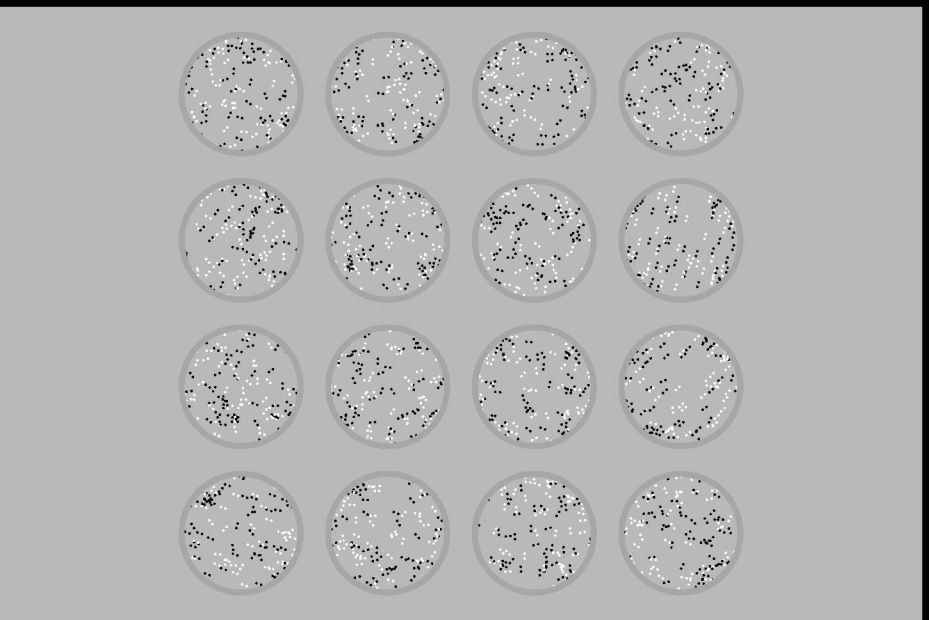

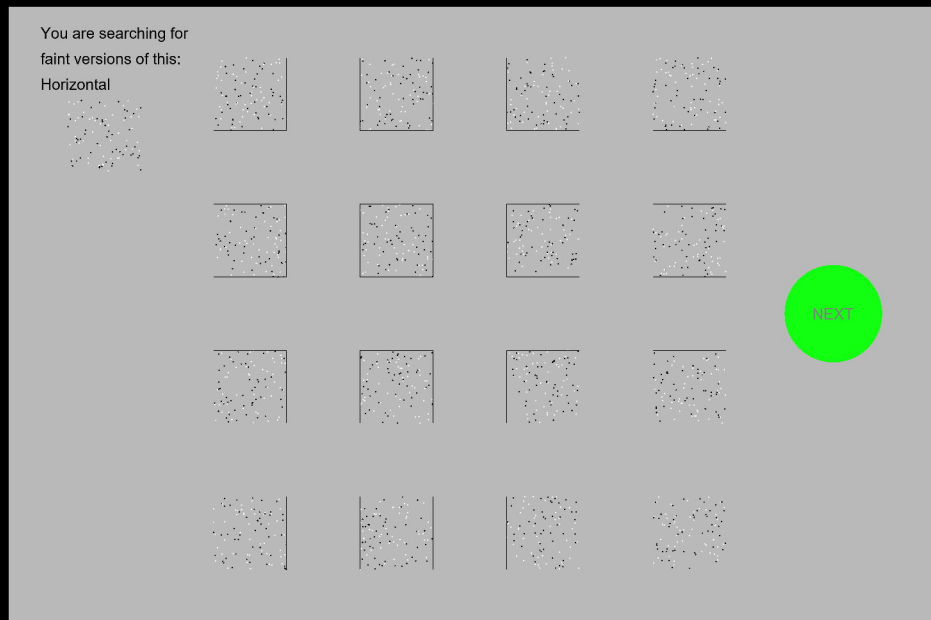
You are searching for
faint versions of this:
Horizontal
NEXT

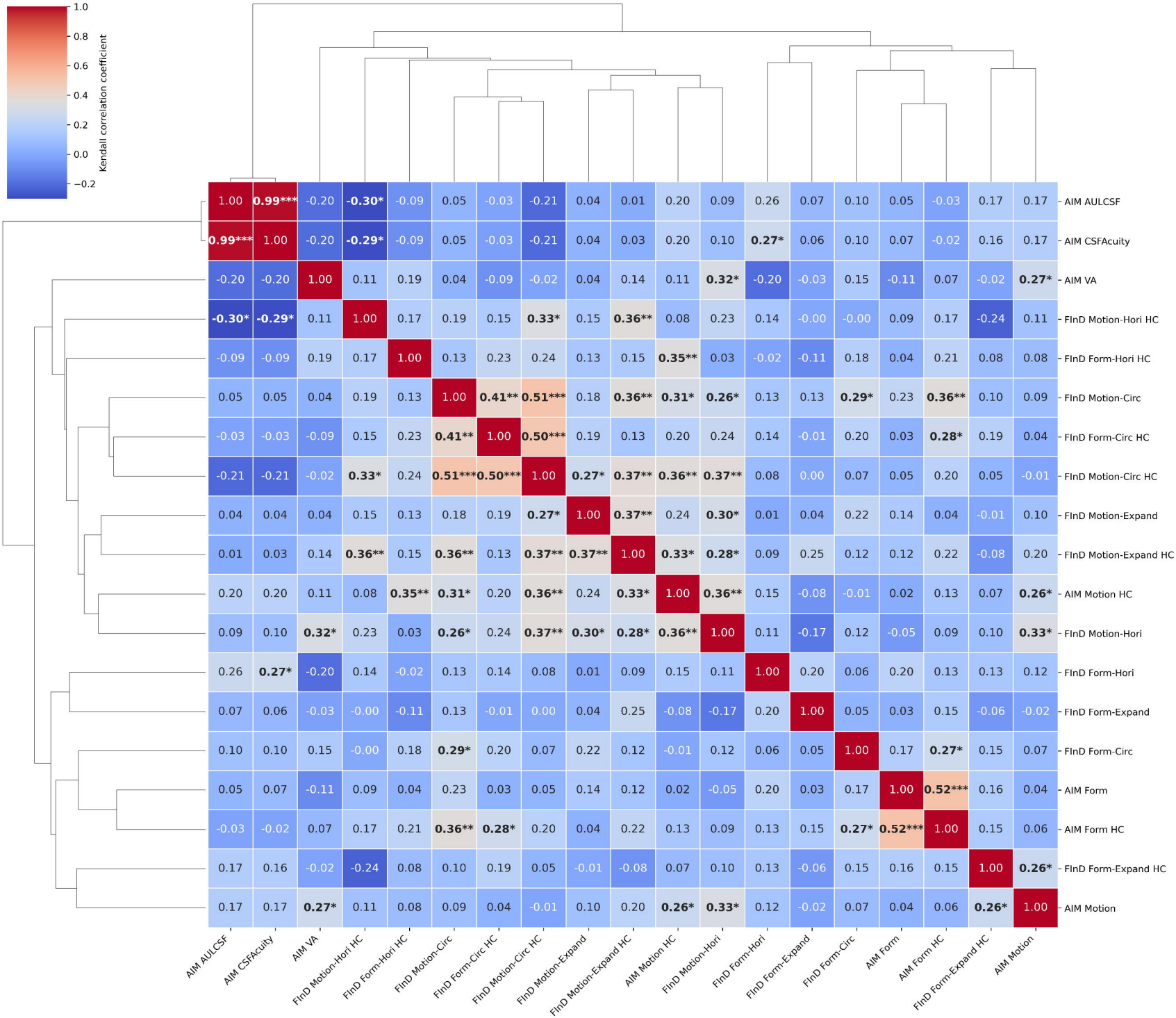
Kendall correlation coefficient
1.0
0.8
0.6
0.4
0.2
0.0
−0.2
AIM AULCSF
AIM CSFAcuity
AIM VA
FInD Motion-Hori HC
FInD Form-Hori HC
FInD Motion-Circ
FInD Form-Circ HC
FInD Motion-Circ HC
FInD Motion-Expand
FInD Motion-Expand HC
AIM Motion HC
FInD Motion-Hori
FInD Form-Hori
FInD Form-Expand
FInD Form-Circ
AIM Form
AIM Form HC
FInD Form-Expand HC
AIM Motion

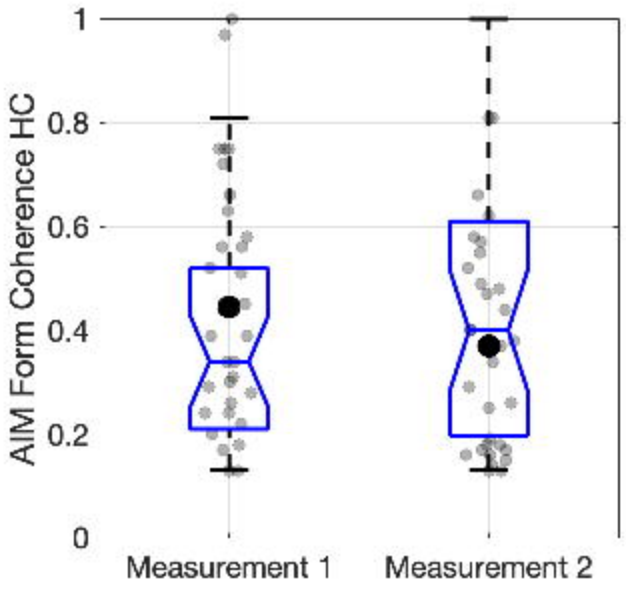
AIM Form Coherence HC
1
0.8
0.6
0.4
0.2
0
Measurement 1
Measurement 2

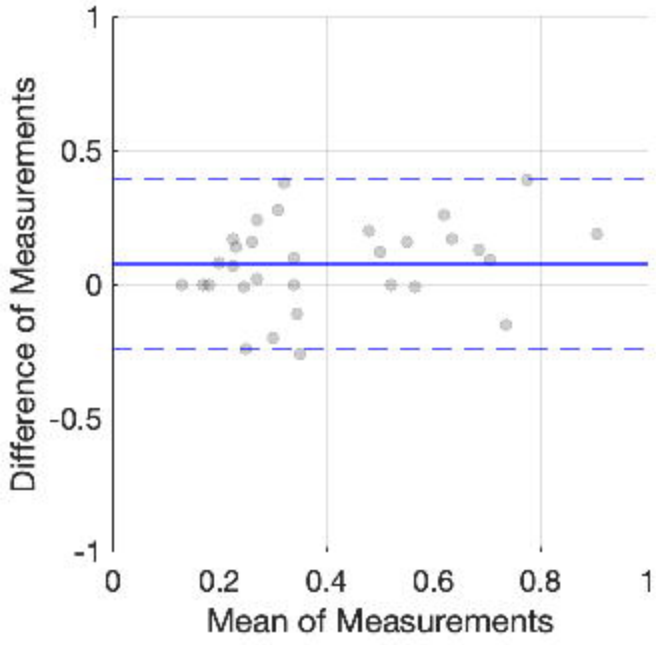
Difference of Measurements
1
0.5
0
-0.5
-1
0
0.2
0.4
0.6
0.8
1
Mean of Measurements

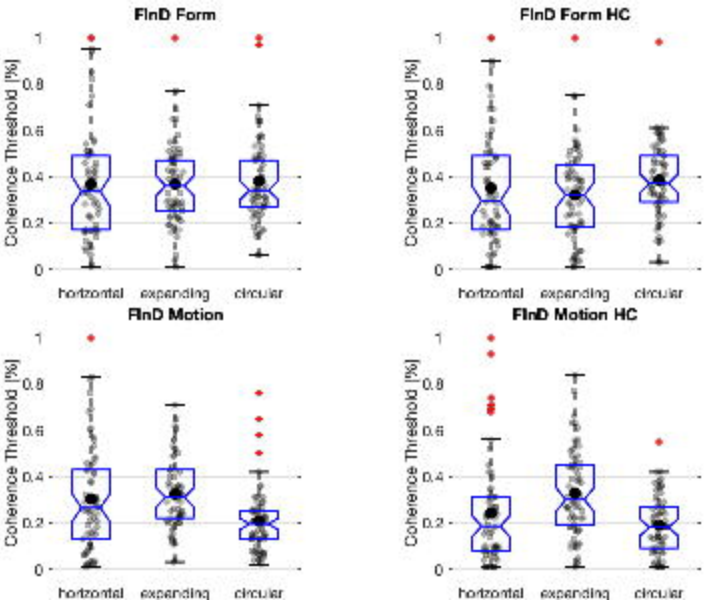
FInD Form
FInD Form HC
FInD Motion
FInD Motion HC
Coherence Threshold [%]
0
0.2
0.4
0.6
0.8
1
horizontal
expanding
circular